nature COMMUNICATIONS

ARTICLE

https://doi.org/10.1038/s41467-021-26038-9 OPEN

闪蒸焦耳热城市采矿

Urban mining by flash Joule heating

Bing Deng[1], Duy Xuan Luong[1], Zhe Wang[1], Carter Kittrell[1], Emily A. McHugh[1] & James M. Tour[1,2,3,4]✉

从电子废物中回收贵金属，称为城市采矿，对循环经济很重要。目前的城市采矿方法，主要是冶炼和浸出，受到漫长的净化过程和不利的环境影响。在此，公开了一种通过快速焦耳加热的无溶剂可持续工艺，以在1秒内回收贵金属并去除电子废物中的有害重金属。通过超快电热过程，样品温度在毫秒内上升到约3400 K。这样的高温使贵金属能够从支撑基质中蒸发分离，铑、钯、银的回收率>80%，金的回收率>60%。电子废物中的重金属（其中一些具有剧毒，包括Cr、As、Cd、Hg和Pb）也被去除，最终的废物金属含量最低，即使在农业土壤水平上也是可以接受的。与使用传统冶炼炉回收金属成分和更环保相比，采用闪光焦耳加热的城市采矿将减少80×至500×的能耗。

Precious metal recovery from electronic waste, termed urban mining, is important for a circular economy. Present methods for urban mining, mainly smelting and leaching, suffer from lengthy purification processes and negative environmental impacts. Here, a solvent-free and sustainable process by flash Joule heating is disclosed to recover precious metals and remove hazardous heavy metals in electronic waste within one second. The sample temperature ramps to ~3400 K in milliseconds by the ultrafast electrical thermal process. Such a high temperature enables the evaporative separation of precious metals from the supporting matrices, with the recovery yields >80% for Rh, Pd, Ag, and >60% for Au. The heavy metals in electronic waste, some of which are highly toxic including Cr, As, Cd, Hg, and Pb, are also removed, leaving a final waste with minimal metal content, acceptable even for agriculture soil levels. Urban mining by flash Joule heating would be 80× to 500× less energy consumptive than using traditional smelting furnaces for metal-component recovery and more environmentally friendly.

---

[1] Department of Chemistry, Rice University, Houston, TX 77005, USA. [2] Smalley-Curl Institute, Rice University, Houston, TX 77005, USA. [3] NanoCarbon Center and the Welch Institute for Advanced Materials, Rice University, Houston, TX 77005, USA. [4] Department of Materials Science and NanoEngineering, Rice University, Houston, TX 77005, USA. ✉email: tour@rice.edu

全球每年产生4000多万吨电子废物，由于个人电气和电子设备的快速升级，电子废物是固体废物中增长最快的组成部分。 More than 40 million tons of electronic waste (e-waste) are produced globally each year[1,2], which is the fastest-growing component of solid wastes due to the rapid upgrade of personal electrical and electronic equipments[3,4]. 大多数电子垃圾都是填埋的，只有约20%被回收利用，由于电子产品中重金属的广泛使用，这可能会对环境造成负面影响。 Most e-waste is landfilled with only ~20% being recycled[5], which could lead to negative environmental impact due to the broad use of heavy metals in electronics[6–8]. 电子垃圾可能成为一种可持续的资源，因为它含有大量有价值的金属。 E-waste could become a sustainable resource because it contains abundant valuable metals[9]. 电子废物中某些贵金属的浓度高于矿石1。从电子废物中回收贵金属，称为城市采矿，比原始采矿更具成本效益，对循环经济也很重要。 The concentrations of some precious metals in e-waste are higher than those in ores[1]. Precious metals recovery from e-waste, termed urban mining, is becoming more cost-effective than virgin mining[2] and important for a circular economy[8]. 同样，由于重金属在电子产品中的广泛使用，包括镉、钴、铜、镍、铅和锌，电子废物可能会导致严重的健康风险和负面环境影响。 Similarly, due to the broad use of heavy metals in electronics, including Cd, Co, Cu, Ni, Pb, and Zn, e-waste could lead to significant health risks and negative environmental impact[6–8]. 垃圾填埋处置不当导致的重金属泄漏导致环境破坏。 The heavy metal leakage due to improper landfill disposal leads to environmental disruption[1,8]. 在回收过程中，有害成分以粉尘或烟雾的形式释放会恶化回收工人和当地居民的健康。 The release of hazardous components during the recycling processes in the form of dust or smoke[6] deteriorates the health of recycling workers and local residents. 例如，在电子废物工人的血液中发现了明显更高浓度的铅。 For example, a significantly higher concentration of Pb has been found in the blood of e-waste workers[7,10].

缺乏高产率和环保的回收过程是城市采矿的主要障碍。 The lack of high-yielding and environmentally friendly recovery processes are the main obstacles to urban mining[9]. 电子废物回收的传统方法是基于火法冶金工艺，金属在高温下加热熔化。 The traditional method for e-waste recycling is based on a pyrometallurgy process[11], where metals are melted by heating at high temperature. 火法冶金是能源密集型的，缺乏选择性，需要高品位的原料。火法冶金过程也会产生含有重金属的有害烟雾，尤其是对于那些熔点较低的重金属，如Hg、Cd和Pb。 Pyrometallurgy is energy-intensive, lacks selectivity, and requires high-grade precursors[12]. Pyrometallurgical processes also produce hazardous fumes containing heavy metals, especially for those with low melting points such as Hg, Cd, and Pb[9]. 湿法冶金工艺更具选择性，通过使用酸、碱或氰化物浸出金属来完成。 The hydrometallurgical process is more selective and done by leaching the metals using acid, base, or cyanide[13]. 浸出动力学通常很慢。 The leaching kinetics are usually slow. 使用高浓度浸出剂使湿法冶金工艺难以大规模应用，产生大量废液和污泥，可能导致二次污染。 The use of highly concentrated leaching agents renders the hydrometallurgical process difficult for large-scale applications, and large amounts of liquid waste and sludge are produced that could result in secondary pollution[14]. 生物冶金可能具有高度选择性和环境可持续性，但它仍处于起步阶段。 Biometallurgy could be highly selective and environmentally sustainable, yet it is still in its infancy[15]. 从各种材料基质（包括塑料、玻璃和陶瓷）中分离有价金属是基于其物理或化学性质的差异。 The separation of valuable metals from various materials matrices, including plastics, glass, and ceramics, are based upon their differences in physical or chemical properties. 例如，重力分离技术依赖于不同的比密度。 For example, the gravity separation technique relies on differing specific densities[16]. 磁选用于从有色金属废料中分离磁性金属。 Magnetic separation is used to separate magnetic metals from non-ferrous waste[17]. 湿法冶金分离基于金属与浸出剂的化学反应。 Hydrometallurgical separation is based upon the chemical reactivity of metals with leaching agents[18].

在这里，我们表明，与基材（碳、陶瓷和玻璃）相比，金属的蒸气压不同，从而能够从电子废物中分离金属。 Here, we show that the different vapor pressure of metals compared to that of substrate materials (carbon, ceramics, and glass) enables the separation of metals from e-waste. 这被称为蒸发分离。 This is termed evaporative separation. 贵金属的高蒸气压是通过真空下的超快闪光焦耳加热（FJH）过程获得的。 The high vapor pressure of precious metals is obtained by an ultrafast flash Joule heating (FJH) process under vacuum. 亚秒电流脉冲通过前体，使样品达到约3400K的超高温，从而实现贵金属的蒸发分离。 A subsecond current pulse is passed through the precursors, which brings the sample to an ultrahigh temperature of ~3400 K, enabling the evaporative separation of precious metals. 使用卤化物添加剂可将Rh、Pd和Ag的回收率提高到80%以上，将被测电子废物中富含的Au的回收率提高到60%以上。 Halide additives are used to improve the recovery yield to >80% for Rh, Pd, and Ag, and >60% for Au that are abundant in the tested e-waste. 或者，与直接浸出电子废物原料相比，通过FJH后的残余固体浸出，回收率显著提高，Ag增加数十倍，Rh、Pd和Au增加几倍。 Alternatively, compared with directly leaching e-waste raw materials, by leaching the residual solids after FJH, the recovery yield is significantly improved with tens of times increase for Ag and few times increase for Rh, Pd, and Au. 有毒重金属，包括Cd、Hg、As、Pb和Cr，也可以去除和收集，从而将回收过程的健康风险和环境影响降至最低。 The toxic heavy metals, including Cd, Hg, As, Pb, and Cr, could also be removed and collected, minimizing the health risks and environmental impact of the recycling process.

结果
Results

FJH从电子废物中蒸发分离贵金属。

Evaporative separation of precious metals from e-waste by FJH. FJH从电子废物中回收贵金属的过程包括三个阶段（图1a）。 The FJH process to recover precious metals from e-waste involves three stages (Fig. 1a). 对电子垃圾中的金属进行加热通过超高温FJH蒸发，然后在真空下传输金属蒸汽并通过冷凝收集。 The metals in e-waste were heated and evaporated by ultrahigh-temperature FJH, then the metal vapors were transported under vacuum and collected by condensation. 废弃计算机的印刷电路板（PCB）是一种典型的电子废弃物，用作起始材料（图1b和补充图1）。 A printed circuit board (PCB) from a discarded computer, a representative e-waste, was used as the starting material (Fig. 1b and Supplementary Fig. 1). 将PCB研磨成小粉末，并与作为导电添加剂的炭黑（CB）混合（图1b，插图）。 The PCB was ground to small powder and mixed with carbon black (CB), which served as the conductive additive (Fig. 1b, inset). 为了确定基准浓度，使用稀释王水溶解PCB，并通过电感耦合等离子体质谱（ICP-MS）测定贵金属的浓度。 To establish baseline concentrations, the PCB was digested using dilute aqua regia[19], and the concentration of precious metals was determined by inductively coupled plasma mass spectrometry (ICP-MS). 在贵金属中，Rh、Pd、Ag和Au含量丰富，浓度为百万分之几到几十（ppm）（图1c）。 Among the precious metals, Rh, Pd, Ag, and Au are abundant with concentrations of several to tens of parts per million (ppm) (Fig. 1c).

在典型的FJH工艺中，PCB粉末和约30 wt%CB的混合物在两个密封电极之间的石英管内被轻微压缩（图1a和补充图2）。 In a typical FJH process, the mixture of PCB powder and ~30 wt% CB was slightly compressed inside a quartz tube between two sealed electrodes (Fig. 1a and Supplementary Fig. 2). 一个电极是多孔铜电极，以促进气体扩散，另一个是石墨棒（补充图3）。 One electrode was a porous Cu electrode to facilitate gas diffusion, and the other was a graphite rod (Supplementary Fig. 3). 通过调节两个电极上的压缩力，可以调节样品的电阻。 The resistance of the sample was tunable by adjusting the compressive force on the two electrodes. 将两个电极连接到总电容为60mF的电容器组上（补充图3）。 The two electrodes were connected to a capacitor bank with a total capacitance of 60 mF (Supplementary Fig. 3). 详细分离条件见补充表1。 The detailed separation conditions are shown in Supplementary Table 1. 电容器组的高压放电使反应物达到高温。 The high-voltage discharge of the capacitor bank brings the reactant to a high temperature. 在固定样品电阻约为1Ω的情况下，在不同FJH电压下测量通过样品的电流（图1d）。 With the fixed sample resistance of ~1 Ω, the current passing through the sample was measured under different FJH voltages (Fig. 1d). 通过拟合600-1100nm发射中的黑体辐射来估计样品的实时温度（补充图4）。 The real-time temperature of the sample was estimated by fitting the blackbody radiation in the 600–1100 nm emission (Supplementary Fig. 4). 温度随FJH电压的变化而变化，在小于50ms的150V下达到3400K左右（图1e）。 The temperature varied according to the FJH voltage, reaching ~3400 K at 150 V in <50 ms (Fig. 1e). 由于样品的电阻远大于石墨和多孔铜电极的电阻，电压降主要施加在样品上。 Since the resistance of the sample is much larger than that of the graphite and porous Cu electrode, the voltage drop was mainly imposed on the sample. 因此，高温区域仅限于样品，FJH装置具有良好的耐久性，即使其可达到>3000K的高温（补充图5）。 Hence, the high-temperature region was limited to the sample and the FJH setup has good durability even though it can achieve a high temperature of >3000 K (Supplementary Fig. 5). 数值模拟表明，样品纵向和径向的温度相对均匀（补充注1，温度模拟，补充图6），证明了FJH工艺的均匀加热能力。 Numerical simulations showed that the temperature was relatively uniform along both the longitudinal and radial directions of the sample (Supplementary Note 1, temperature simulation, Supplementary Fig. 6), demonstrating the homogenous heating ability of the FJH process.

这样的高温（>3000K）会挥发大部分非碳成分。 Such a high temperature (>3000 K) volatilizes most of the non-carbon components. 根据计算的蒸气压-温度关系（图1f），贵金属的蒸气压高于碳，后者直到3900K左右才升华。 According to the calculated vapor pressure–temperature relationships (Fig. 1f), the precious metals have a higher vapor pressure than carbon, the latter not subliming until ~3900 K[20]. 结果，金属被蒸发，塑料等主要含碳成分被碳化。 As a result, the metals are evaporated, and the major carbon-containing components such as plastics were carbonized[21,22]. 蒸发的金属蒸汽通过冷阱中的冷凝被捕获（图1a和补充图2）。 The evaporated metal vapors were captured by condensation in a cold trap (Fig. 1a and Supplementary Fig. 2). 即使在液氮温度（77K）下，一些蒸汽仍保持气态（补充图2）；这些气体被假定为H2和CO2。 Some of the vapor remained gaseous even at the liquid N_2 temperature (77 K) (Supplementary Fig. 2); these gases were presumed to be H_2 and CO[22]. 测量浓缩固体中贵金属的含量，并计算回收率（图1g和补充注释2）。 The content of the precious metals in the condensed solid was measured and the recovery yield was calculated (Fig. 1g and Supplementary Note 2). 银的回收率约为40%，而铑、钯和金的回收率相对较低，约为3%。 The recovery yield of Ag was ~40%, while Rh, Pd, and Au had a relatively low recovery yield of ~3%. 这是因为银具有较高的蒸汽压和相对较低的沸点（补充图7）。 This is because Ag has a high vapor pressure and relatively low boiling point (Supplementary Fig. 7). 起始商业炭黑中的贵金属浓度为PCB中浓度的1.2%，因此它们在炭黑中的存在不会产生重大误差（补充图8）。 The concentration of precious metals in the starting commercial CB is 1–2% of the concentration in PCB, hence their presence in CB will not introduce significant errors (Supplementary Fig. 8). 此外，贵金属由于其极低的C溶解度，即使在高温下也不会形成稳定的碳化物相（补充图9）。 Moreover, the precious metals tend to not form stable carbide phases even at high temperature due to their extremely low C solubility[23] (Supplementary Fig. 9). 因此，将炭黑用作导电添加剂不会影响贵金属的蒸发行为。 Hence, the use of CB as a conductive additive will not affect the evaporative behavior of precious metals.

卤化物有助于提高回收率。

Halide assisted improvement of recovery yield. 蒸发分离的高回收率依赖于产生更多挥发性成分。 The high-recovery yield of the evaporative separation relies on the

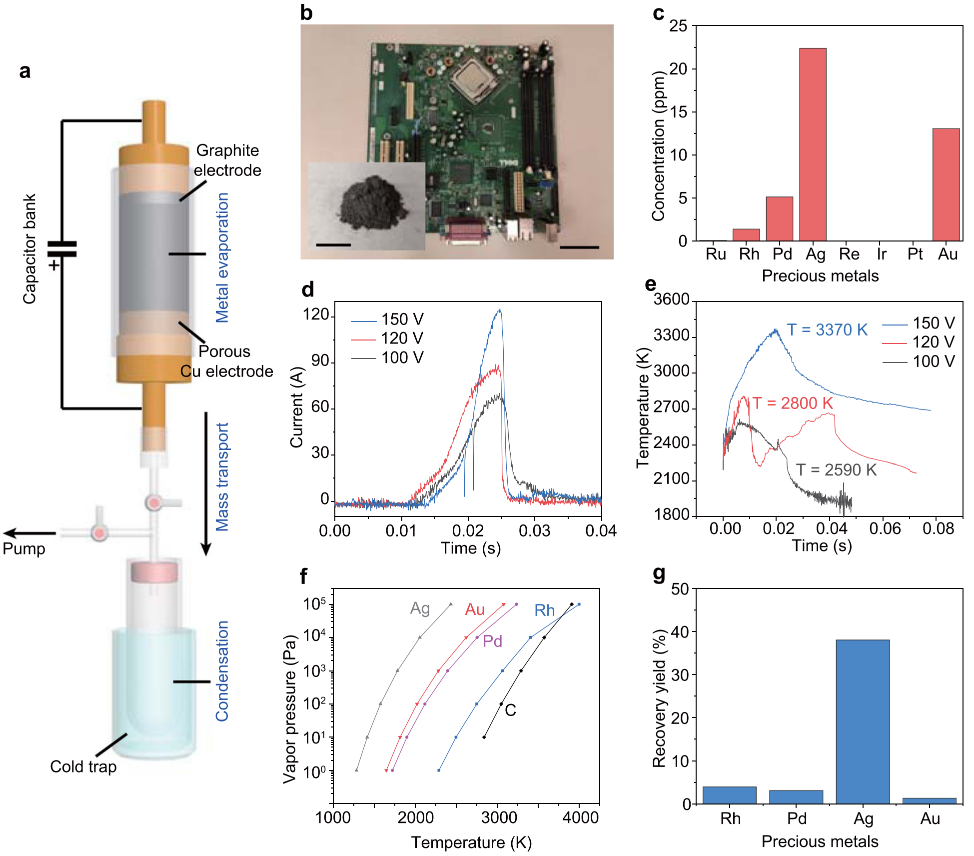

Fig. 1 Recovery of precious metals by flash Joule heating (FJH). a Schematic of the FJH and evaporative separation system. The system was composed of three parts, including FJH for metal evaporation, the vacuum system for mass transport, and the cold trap for volatiles condensation. **b** Picture of a printed circuit board (PCB). Scale bar, 5 cm. Inset, the mixture of carbon black (CB) with PCB powder. Scale bar, 2 cm. **c** Concentrations of precious metals in PCB as determined by inductively coupled plasma mass spectrometry (ICP-MS). **d** Currents vs time recorded under different FJH voltages. **e** Real-time temperature measurements at different FJH voltages by fitting blackbody radiation emitted from the sample. **f** Vapor pressure–temperature relationship of precious metals and carbon. **g** Recovery yield of precious metals by condensing the evaporated gas components. The recovery yield is the average of three independent FJH experiments ($n = 3$).

图1：通过快速焦耳加热(FJH)回收贵金属。FJH和蒸发分离系统示意图。该系统由三部分组成，包括用于金属蒸发的FJH、用于质量传输的真空系统和用于挥发物冷凝的冷阱。b、印刷电路板(PCB)的图片。比例尺，5cm。插图，炭黑(CB)与PCB粉末的混合物。比例尺，2cm。c、通过电感耦合等离子体质谱(ICP-MS)测定PCB中贵金属的浓度。d、不同FJH电压下记录的电流与时间。通过拟合样品发出的黑体辐射，实时测量不同FJH电压下的温度。贵金属和碳的蒸气压-温度关系。g、通过冷凝蒸发气体成分回收贵金属。回收率是三个独立FJH试验(n=3)的平均值。

generation of more volatile components. To improve the recovery, halides were used as additives because of the much higher vapor pressure of metal halides compared with the elemental metals (Supplementary Fig. 10)[24]. Fluorine-containing components were first used as the additive, including sodium fluoride (NaF) and polytetrafluoroethylene (PTFE, Teflon). With the additives, the recovery yields of Rh and Pd were improved to >80% and 70%, respectively (Fig. 2a, b and Supplementary Note 2), demonstrating ~20× improvement compared to the experiments without additives. The concentration of precious metals in the additives was <2% of those in PCB (Supplementary Fig. 11), hence we can exclude the additives from introducing significant error in the recovery of precious metals. Chlorine-containing compounds were tried because of their abundance and low cost. Both sodium chloride (NaCl) and potassium chloride (KCl) were used (Fig. 2c and Supplementary Fig. 12). The recovery yields of Rh, Pd, and Ag increased for both NaCl and KCl additives. In addition, both polyvinyl chloride (PVC) and chlorinated polyvinyl chloride (CPVC) plastics were used (Fig. 2d and Supplementary Fig. 12). The recovery yield of all four precious metals was increased, especially for Ag, with the recovery yield improving to >80%. The plastic additives were ground post-consumer samples with very low or negative values, so they will not introduce significant materials cost during the e-waste recycling process.

为了提高回收率，使用卤化物作为添加剂，因为金属卤化物的蒸气压比元素金属高得多(补充图10)24。首先使用含氟成分作为添加剂，包括氟化钠(NaF)和聚四氟乙烯(PTFE、Teflon)。使用添加剂后，Rh和Pd的回收率分别提高到80%和70%以上(图2a、b和补充注释2)，与不使用添加剂的实验相比，提高了约20倍。添加剂中的贵金属浓度<PCB中贵金属浓度的2%(补充图11)，因此我们可以排除添加剂在贵金属回收中引入的重大误差。含氯化合物因其含量丰富、成本低廉而被尝试。使用氯化钠(NaCl)和氯化钾(KCl)(图2c和补充图12)。NaCl和KCl添加剂的Rh、Pd和Ag的回收率均增加。此外，还使用了聚氯乙烯(PVC)和氯化聚氯乙烯(CPVC)塑料(图2d和补充图12)。四种贵金属的回收率都有所提高，尤其是银，回收率提高到80%以上。塑料添加剂是消费后研磨的样品，其值非常低或为负值，因此在电子废物回收过程中不会产生重大的材料成本。

Even with the F and Cl additives, the recovery yield of Au is <10%. Interestingly, the recovery yields of all four precious metals were improved when sodium iodide (NaI) was used as the additive; the recovery yield of Au was improved to >60% (Fig. 2e). The I additive has the best performance among halides for Au recovery. According to the hard and soft acids and bases (HSAB) theory, Au$^+$ is a soft Lewis acid, and I^- is a soft Lewis base while F^- and Cl^- are harder than I^-[25], favoring AuI. By using an additive mixture of NaF, NaCl, and NaI, the precious metals all had a good recovery yield, >60% for Rh, >60% for Pd, >80% for Ag, and >40% for Au (Fig. 2f). The composition analysis of the raw materials and the remaining solid after FJH by X-ray photoemission spectroscopy (XPS) showed that 10–40% of the halide additives were evaporated during the FJH process (Supplementary Fig. 13), which could be recovered and reused by a water washing and precipitation process.

即使使用F和Cl添加剂，金的回收率也小于10%。有趣的是，当使用碘化钠(NaI)作为添加剂时，所有四种贵金属的回收率都得到了提高；金的回收率提高到60%以上(图2e)。在卤化物中，I添加剂的金回收性能最好。根据硬和软酸碱(HSAB)理论，Au+是软Lewis酸，I是软Lewis碱，而F和Cl比I 25硬，有利于AuI。通过使用NaF、NaCl和NaI的添加剂混合物，贵金属都具有良好的回收率，Rh>60%，Pd>60%，Ag>80%，Au>40%(图2f)。通过X射线光电子能谱(XPS)对原材料和FJH后剩余固体的成分分析表明，FJH过程中蒸发了10-40%的卤化物添加剂(补充图13)，可通过水洗和沉淀过程回收和再利用。

We conducted a total composition analysis of the collected metals in the cold trap (Supplementary Note 3). In both cases with or without the chemical additives, in addition to the precious metals, the most abundant metals were Cu with mass ratio >60 wt %, followed by other prominent metals in e-waste including Al, Sn, Fe, and Zn (Supplementary Fig. 14). Further purification and refining could be done by selective precipitation, solvent extraction, and solid-phase extraction, which are commercially well-established practices[26].

我们对冷阱中收集的金属进行了总成分分析(补充注3)。在有无化学添加剂的两种情况下，除贵金属外，最丰富的金属是铜，质量比>60 wt%，其次是电子废物中的其他主要金属，包括铝、锡、铁和锌(补充图14)。进一步的提纯和精炼可以通过选择性沉淀、溶剂萃取和固相萃取来完成，这些都是商业上公认的做法。

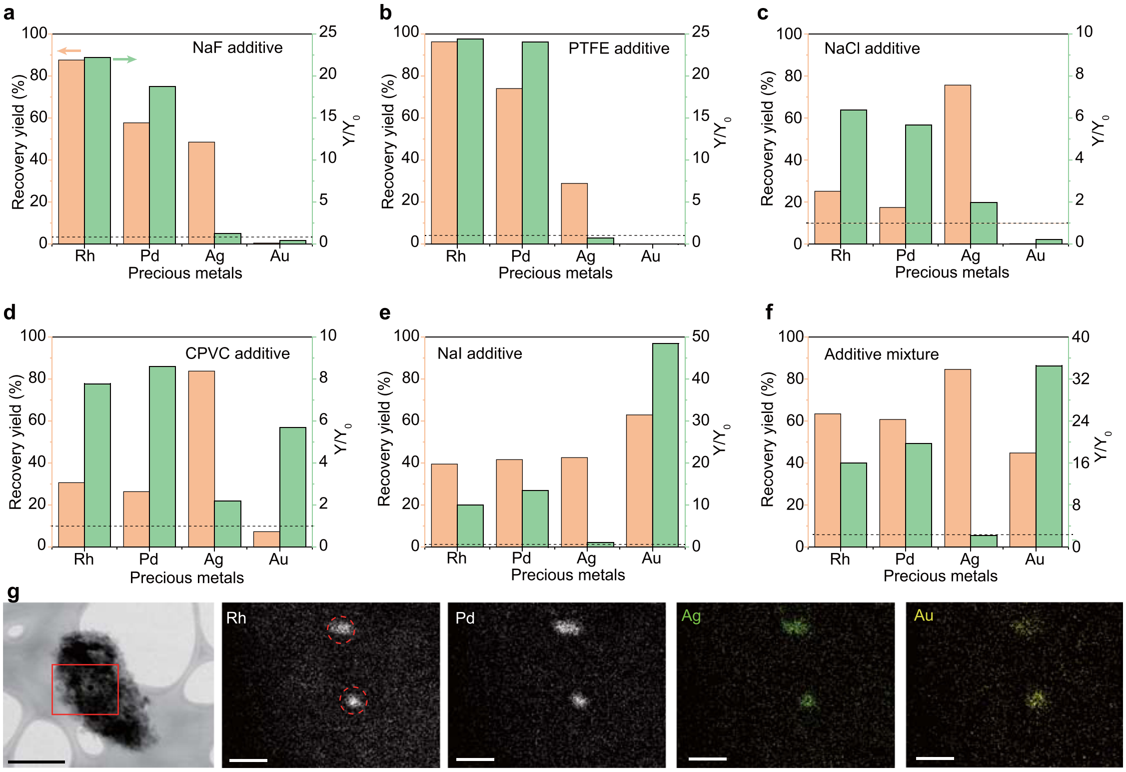

Fig. 2 Halide assisted improvement of recovery yield. Recovery yield of precious metals by using (**a**) NaF, (**b**) PTFE, (**c**) NaCl, (**d**) CPVC, (**e**) NaI, and (**f**) mixture of NaF, NaCl, and NaI, as additives. Y_0 and Y mean the recovery yield of precious metals without and with additives, respectively. The dashed line denotes $Y/Y_0 = 1$, meaning that there is no advantage of the additive if $Y/Y_0 \leq 1$. The recovery yields were the average of three independent flash Joule heating (FJH) experiments ($n = 3$). **g** Scanning transmission electron microscopy (STEM) image of the collected solids, and energy dispersive spectroscopy (EDS) maps of Rh, Pd, Ag, and Au at the rectangular region. Scale bar in STEM image, 0.5 μm; scale bars in EDS maps, 100 nm. The dashed circles in Rh show the clustered alloys.

图2 卤化物辅助提高回收率。使用(a)NaF、(b)PTFE、(c)NaCl、(d)CPVC、(e)NaI和(f)NaF、NaCl和NaI混合物作为添加剂，回收贵金属的收率。Y0和Y分别表示不添加和添加添加剂时贵金属的回收率。虚线表示Y/Y0=1，这意味着如果Y/Y0为1，则添加剂没有优势。回收率是三次独立闪光焦耳加热(FJH)实验(n=3)的平均值。g、收集的固体g扫描透射电子显微镜(STEM)图像，以及矩形区域的Rh、Pd、Ag和Au的能量色散光谱(EDS)图。STEM图像中的比例尺，0.5 μm；EDS地图中的比例尺，100nm。右侧的虚线圆圈表示聚集的合金。

The morphology and chemical composition of the condensed solids were characterized using scanning transmission electron microscopy (STEM) and energy dispersion spectroscopy (EDS). The elemental maps showed the clustered alloy particles of Rh, Pd, Ag, and Au (Fig. 2g), which were formed by the ultrafast heating and rapid cooling of the FJH process. This is similar to the case of the carbothermic shock synthesis of high-entropy alloy nanoparticles, which could be potentially used in catalysts[27]. In other regions, the precious metals spreading over the entire product were also observed (Supplementary Fig. 15). Moreover, the XPS analysis of the collected volatiles showed that Ag and Au were mainly in the elemental state, while elemental state and higher oxidation state coexisted for Rh and Pd, presumably due to their different chemical reactivity (Supplementary Note 3 and Supplementary Fig. 16).

使用扫描透射电子显微镜(STEM)和能量色散光谱(EDS)对凝聚固体的形态和化学成分进行了表征。元素图显示了Rh、Pd、Ag和Au的聚集合金粒子(图2g)，这些粒子是通过FJH工艺的超快加热和快速冷却形成的。这类似于碳热冲击合成高熵合金纳米颗粒的情况，该纳米颗粒可能用于催化剂。在其他地区，也观察到贵金属遍布整个产品(补充图15)。此外，收集挥发物的XPS分析表明，Ag和Au主要处于元素状态，而Rh和Pd的元素状态和更高氧化状态共存，这可能是由于其不同的化学反应性(补充注释3和补充图16)。

提高了FJH对贵金属的浸出效率。

Improved leaching efficiency of precious metals by FJH. Apart from the condensation of the volatile composition, the other pathway to recover the precious metals was by leaching the residual solids obtained by FJH (Supplementary Fig. 17a). Different from the use of a vacuum to facilitate the metal volatilization in the evaporative separation scheme (Fig. 1a), a pressurized setup was built to trap the metals in the reactor (Fig. 3a). An inert gas (N_2) cylinder was connected to the FJH reactor, where the pressure was monitored by a pressure gauge. The inner pressure (P_0) during FJH was estimated to be ~5 atm according to the amount of collected gas (Supplementary Fig. 2 and Supplementary Note 1). Based on the pressure drop and the size of the FJH chamber, the gas diffusion was simulated under different pressures (P_{out}) (Fig. 3b, Supplementary Fig. 18). When vacuum was used ($P_{out} = 0$ atm), as it is in the evaporative separation (Fig. 1a), the gas velocity was up to 800 m s^{-1}. Such a high gas velocity aided the volatile components to quickly diffuse to the cold trap and prevent the condensation loss at the tube sidewalls. In contrast, the gas velocity was greatly reduced with the increase in pressure (Fig. 3b). As a result, more of the originally volatile components were trapped within the residual solids in the reactor. The detailed reaction conditions for the pressurized FJH are shown in Supplementary Table 2.

除了挥发性成分的冷凝之外，回收贵金属的另一个途径是通过浸出FJH获得的残余固体(补充图17a)。与蒸发分离方案(图1a)中使用真空促进金属挥发不同，建立了加压装置以捕获反应器中的金属(图3a)。惰性气体(N2)钢瓶连接至FJH反应器，压力由压力计监测。根据收集的气体量，FJH期间的内压(P0)估计约为5 atm(补充图2和补充注释1)。根据FJH燃烧室的压降和尺寸，模拟了FJH燃烧室中气体的扩散过程不同压力(Pout)(图3b，补充图18)。当使用真空(Pout=0atm)时，正如在蒸发分离中一样(图1a)，气体速度高达800m/s。如此高的气体流速有助于挥发性成分迅速扩散到冷阱中，并防止管侧壁处的冷凝损失。相反，随着压力的增加，气体速度大大降低(图3b)。结果，更多原本易挥发的成分被困在反应器中的残余固体中。加压FJH的详细反应条件见补充表2。

We started from leaching the residual solids after FJH (denoted as PCB-Flash) at 120 V and atmospheric pressure using dilute acids (1 M HCl, 1 M HNO_3) (Supplementary Fig. 17a). The leachable content of Rh, Pd, and Ag in PCB-Flash was substantially higher than that in the PCB raw materials (Fig. 3c). The ratio of the recovery yield by leaching the PCB-Flash (Y) and leaching the PCB raw materials (Y_0) was calculated. FJH with leaching was far more effective than leaching alone. The recovery yield of Rh, Pd, and Ag was increased by 4.17 ± 0.48, 2.90 ± 0.31, 56.0 ± 18.1 times, respectively (Fig. 3c). The deviations could be from the inhomogeneous distribution of precious metals in e-waste. Interestingly, the Au recovery yield was reduced after the FJH process. The reason was presumably the formation of covalent bonds between Au and carbon[28], which could significantly increase the difficulty of acid leaching. The thermogravimetric analysis (TGA) of the PCB-Flash showed that the carbon could be removed in the air at ~700 °C (Supplementary Fig. 17b). Hence, the PCB-Flash solid was calcined at 700 °C for 1 h (denoted as PCB-Flash-Calcination, Supplementary

我们从使用稀酸(1 M HCl，1M HNO3)在120V和大气压下FJH(表示为PCB闪蒸)后的残余固体浸出开始(补充图17a)。闪蒸PCB中Rh、Pd和Ag的可浸出含量大大高于PCB原材料中的含量(图3c)。计算了PCB闪蒸浸出回收率(Y)与PCB原料浸出回收率(Y0)的比值。FJH加浸出比单独浸出有效得多。Rh、Pd、Ag的回收率分别提高了4.17±0.48、2.90±0.31，分别为56.0±18.1倍(图3c)。这些偏差可能与电子废物中贵金属的不均匀分布有关。有趣的是，FJH工艺后，金回收率降低。原因可能是Au和碳之间形成共价键，这会显著增加酸浸的难度。PCB闪蒸的热重分析(TGA)表明，在约700°C的温度下，可以去除空气中的碳(补充图17b)。因此，PCB闪蒸固体在700°C下煅烧1h(表示为PCB闪蒸煅烧，补充图17b)。

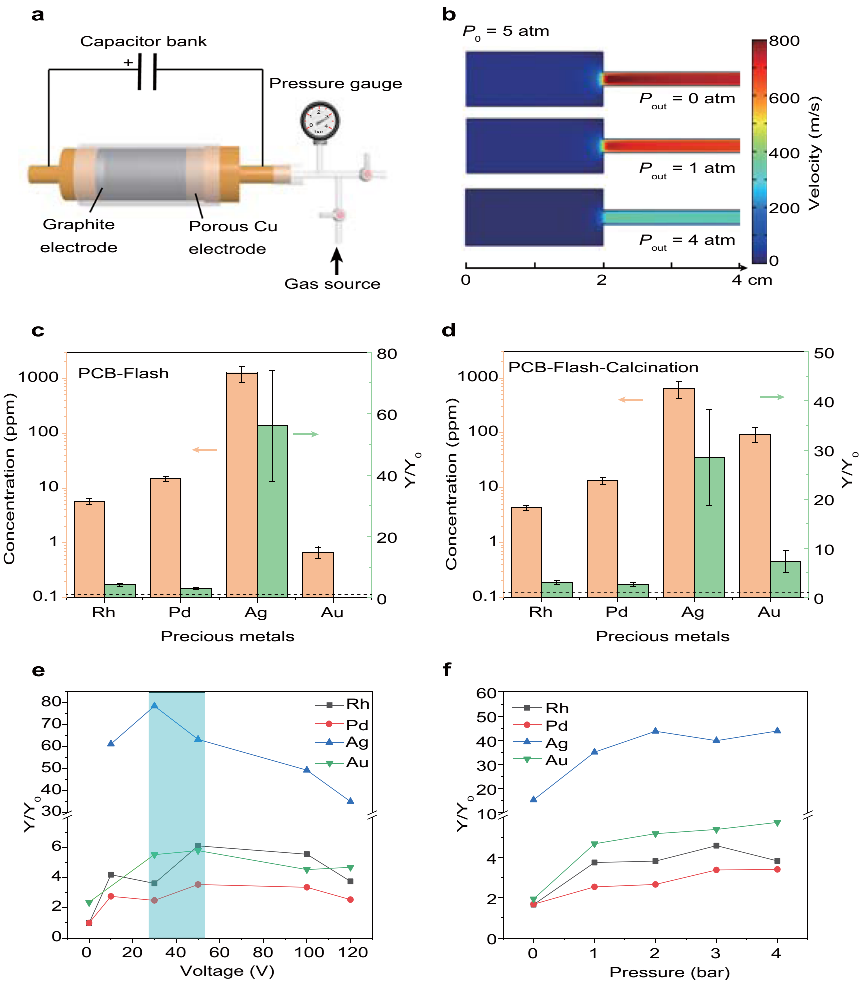

Fig. 3 Leaching efficiency improvement of precious metals by the flash Joule heating (FJH) process. a Schematic of the pressurized setup for FJH. **b** Gas flow simulation under different pressures. The inner pressure (P_O) during the FJH was calculated to be ~5 atm. P_{out} of 0 atm, 1 atm, and 4 atm correspond to the FJH under vacuum, atmospheric pressure, and 3 atm of positive pressure. **c** Concentration of precious metals and improvement of recovery yield by FJH. Y_O and Y mean the recovery yield by leaching printed circuit board (PCB) and PCB-Flash, respectively. The dashed line denotes $Y/Y_O = 1$. The error bars denote the standard deviation where $n = 3$. **d** Concentration of precious metals and improvement of recovery yield by FJH and calcination. Y_O and Y mean the recovery yield by leaching PCB and PCB-Flash-Calcination, respectively. The dashed line denotes $Y/Y_O = 1$. The error bars denote the standard deviation where $n = 3$. **e** Improvement of recovery yield varied with FJH voltages under atmospheric pressure. The highlighted region is the approximate optimal voltage for all metal recovery. **f** Improvement of recovery yield varied with pressure. For **e** and **f**, the recovery yields of Rh, Pd, and Ag are calculated from PCB-Flash, and the recovery yield of Au is calculated from PCB-Flash-Calcination.

图3、闪速焦耳加热(FJH)工艺提高贵金属浸出效率。a、FJH加压设置示意图。b、气体不同压力下的流动模拟。计算出FJH期间的内压(P0)约为5atm。0atm、1atm和4atm的Pout对应于真空、大气压和3atm正压下的FJH。c、通过FJH富集贵金属并提高回收率。Y0和Y分别表示通过浸出印刷电路板(PCB)和PCB闪存获得的回收率。虚线表示Y/Y0=1。误差条表示标准偏差，其中n=3。d、通过FJH和煅烧富集贵金属并提高回收率。Y0和Y分别表示PCB浸出和PCB闪速煅烧的回收率。虚线表示Y/Y0=1。误差条表示标准偏差，其中n=3。在常压下，回收率的提高随FJH电压的变化而变化。突出显示的区域是所有金属回收的近似最佳电压。f、提高采收率随压力变化。对于e和f，Rh、Pd和Ag的回收率通过PCB闪蒸计算，Au的回收率通过PCB闪蒸煅烧计算。

Fig. 17b). The PCB raw materials were also calcined as a control (denoted as PCB-Calcination, Supplementary Fig. 17c). The XPS analysis showed the efficient removal of carbon by calcination (Supplementary Fig. 17d). With the FJH and calcination process, the recovery yields of Rh, Pd, Ag, and Au were increased by 3.11 ± 0.37, 2.64 ± 0.39, 28.5 ± 9.8, 7.24 ± 2.22 times, respectively (Fig. 3d). The values are larger than those achieved with the calcination-only process (Supplementary Figs. 17e, f).

PCB原材料也作为对照进行煅烧(表示为PCB煅烧，补充图17c)。XPS分析表明，通过煅烧可以有效去除碳(补充图17d)。通过FJH和煅烧工艺，Rh、Pd、Ag和Au的回收率分别提高了3.11±0.37、2.64±0.39、28.5±9.8、7.24±2.22倍(图3d)。这些值大于仅通过煅烧工艺获得的值(补充图17d)。

The presumable mechanism of the improved leaching efficiency by FJH is shown in Supplementary Fig. 19. Modern electronics are fabricated and packaged by a planar process and have a laminated configuration, where the useful metals are embedded into the polymer or ceramic matrices (Supplementary Fig. 19a)[13]. Even after the pulverization, the particle size was large ~5 µm (Supplementary Fig. 19b). The laminated structure hinders the extraction of metals in a typical hydrochemical process, resulting in elongated leaching times and low leaching efficiencies[13]. During the FJH process, the matrix was rendered as an ultrafine powder at the ultrahigh temperature (Supplementary Figs. 19c, d), and the metals were exposed (Supplementary Fig. 19e), which greatly accelerated the leaching rate and extent of metal extraction.

FJH提高浸出效率的可能机制如补充图19所示。现代电子器件通过平面工艺制造和封装，并具有层压结构，其中有用金属嵌入聚合物或陶瓷基体中(补充图19a)13。即使在粉碎后，粒径仍较大，约5 μm(补充图19b)。层状结构阻碍了典型水化学过程中金属的提取，导致浸出时间延长，浸出效率低。在FJH过程中，基体在超高温下呈现为超细粉末(补充图19c，d)，作为超高温下的超细粉末并暴露金属(补充图19e)，这大大加快了金属提取的浸出速度和程度。

The effects of the FJH voltage and pressure on the recovery yield were studied. It was found that the modest FJH voltages between 30 and 50 V led to the best recovery yield (Fig. 3e). Too low voltage did not provide enough energy to thermally decompose the matrix, while too high voltage presumably resulted in the evaporative loss. It was found that a higher surrounding pressure was beneficial (Fig. 3f). This is because the volatile components were trapped in the residual solid, as we projected by the gas- flow simulations (Fig. 3b). The mild acid-leaching condition (1 M HCl, 1 M HNO_3) used in our process is more cost-effective and environmentally friendly compared to other hydrometallurgical processes, which use highly concentrated mineral acids such as aqua regia[13,29], or toxic cyanides[18,30] as extractants for achieving a high-recovery yield.

研究了FJH电压和压力对回收率的影响。研究发现，30至50V之间的适度FJH电压可获得最佳的回收率(图3e)。过低的电压不能提供足够的能量来热分解基质，而过高的电压可能会导致蒸发损失。发现较高的环境压力是有益的(图3f)。这是因为挥发性成分被困在残余固体中，正如我们通过气流模拟预测的那样(图3b)。与其他湿法冶金工艺相比，我们工艺中使用的温和酸浸条件(1M HCl、1M HNO3)更具成本效益和环境友好性，其他湿法冶金工艺使用王水13,29或有毒氰化物18,30等高浓度矿物酸作为萃取剂，以实现高回收率。

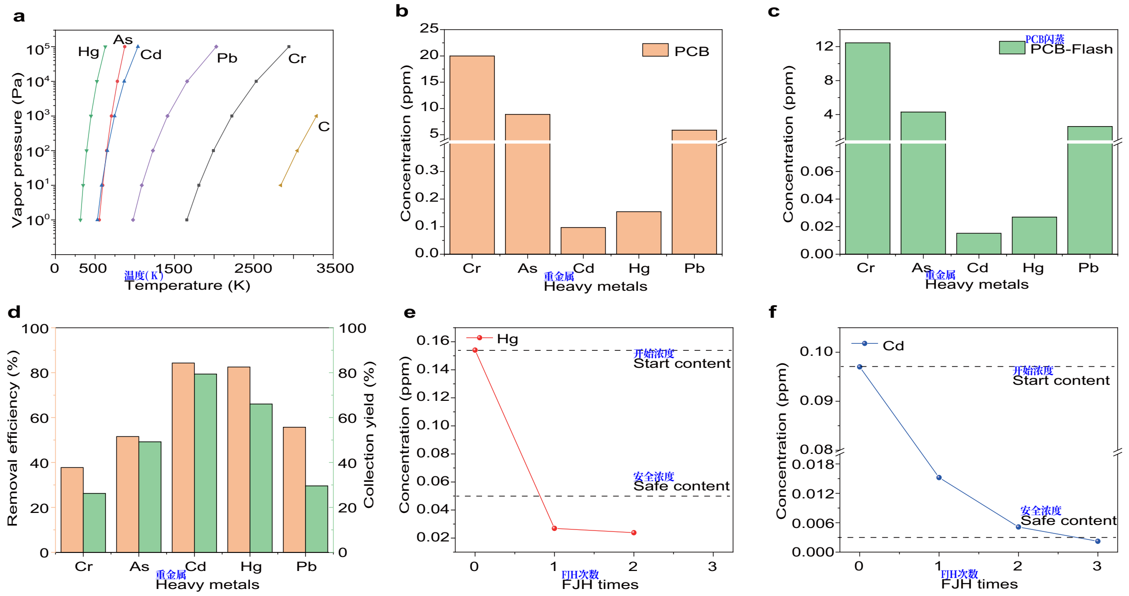

图4、闪速焦耳加热(FJH)工艺去除电子垃圾中的重金属。
Fig. 4 Removal of heavy metals in e-waste by flash Joule heating (FJH) process.
a、碳与有毒重金属的蒸气压-温度关系
a Vapor pressure–temperature relationships of toxic heavy metals and carbon.
b、印刷电路板(PCB)中有毒重金属的浓度。
b Concentrations of toxic heavy metals in the printed circuit board (PCB).
c、FJH后PCB中有毒重金属的浓度。
c Concentrations of toxic heavy metals in PCB after FJH.
d、重金属的去除效率和收集率。
d Removal efficiency and collection yield of heavy metals.
效率和产量是三个独立FJH试验(n=3)的平均值。
The efficiency and yield were the average of three independent FJH experiments ($n = 3$).
e、多次FJH反应后残留物中的汞浓度。
e Concentration of Hg in the residues after multiple FJH reactions.
f、多次FJH反应后残留物中的镉浓度。
f Concentration of Cd in the residues after multiple FJH reactions.
(e、f)中的虚线表示农业土壤安全限值的起始浓度和世界卫生组织(WHO)批准的浓度。
The dashed lines in (**e**, **f**) represent the starting contents and the approved World Health Organization (WHO) level for safe limits of agricultural soils.

去除和收集电子废物中的有毒重金属。

Removal and collection of toxic heavy metals in e-waste.
去除有毒成分是电子废物处理的另一个主要问题3、6、7、31。
Removal of toxic components is another major concern for e-waste processing[3,6,7,31].
对FJH工艺的重金属去除能力进行了评价。
The heavy metal removal capability of the FJH process was evaluated.
与贵金属相比，重金属，包括Cr、Pb、Cd、As和Hg，具有更高的蒸气压和更低的沸点(图4a和补充图7b)。
Compared to precious metals, heavy metals, including Cr, Pb, Cd, As, and Hg, have much higher vapor pressures and lower boiling points (Fig. 4a and Supplementary Fig. 7b).
特别是对于毒性最大的镉、砷和汞，根据理论分析，它们与贵金属之间的分离系数可达到约10^5(补充注4)。
Especially for the most toxic Cd, As, and Hg, the separation factors between them and precious metals could achieve $\sim10^5$ based on the theoretical analysis (Supplementary Note 4).
PCB废物中的重金属含量在0.1-20ppm的范围内(图4b)。
The levels of heavy metals in PCB waste are in the range of 0.1–20 ppm (Fig. 4b).
这些数值高于世界卫生组织(WHO)建议的农业土壤重金属安全限值。
These values are above the safe limits of heavy metals in soils for agriculture as recommended by the world health organization (WHO)[32].
经过一次FJH后，剩余固体(PCB闪蒸)中的重金属含量大大降低(图4c)。
After one FJH, the heavy metal contents in the remaining solid (PCB-Flash) were greatly reduced (Fig. 4c).
经计算，汞和镉的去除效率>80%，其次是铅和砷(>50%)，以及铬(>35%)(图4d和补充注释2)。
The removal efficiencies of Hg and Cd were calculated to be >80%, followed by Pb and As (>50%), and Cr (>35%) (Fig. 4d and Supplementary Note 2).
这些效率与其蒸汽压值一致(图4a)。
These efficiencies were consistent with their vapor pressure values (Fig. 4a).
与蒸发分离一样，通过冷阱中的冷凝收集重金属，并计算收集量(图4d)。
The heavy metals were collected by condensation in the cold trap, as we did for the evaporative separation, and the collection yields were calculated (Fig. 4d).
收集率与去除效率非常匹配，表明大部分蒸发的重金属被冷阱捕获，从而最大限度地减少了重金属在回收过程中泄漏到环境中的情况。
The collection yield matched well with the removal efficiency, demonstrating that most of the evaporated heavy metal was trapped by the cold trap, minimizing the leakage of heavy metals into the environment during the recycling process.

多次FJH反应可进一步降低残渣固体中重金属的浓度。
The concentration of heavy metals in the residue solids could be further reduced by multiple FJH reactions.
经过一次FJH反应后，汞的浓度降低到农业土壤中汞的安全限值(0.05ppm)以下(图4e)，废物处理的最高标准。
After one FJH reaction, the concentration of Hg was reduced to below the safe limit of Hg in soils for agriculture (0.05 ppm) (Fig. 4e)[32], the highest standard for waste disposal.
对于Cd，连续三次FJH循环将浓度降低到安全限值(0.003 ppm)以下(图4f)。
As for Cd, three consecutive FJH cycles reduced the concentration to below the safe limit (0.003 ppm) (Fig. 4f)[32].
随着FJH反应次数的增加，As、Pb和Cr的浓度均降低(补充图20)。
The concentration of As, Pb, and Cr were all reduced with an increase in the number of FJH reactions (Supplementary Fig. 20).
由于每次FJH只需1s，因此可以轻松完成多次闪蒸。
Since each FJH only takes 1 s, multiple flashes are easily accomplished.

讨论
Discussion

设计的蒸发分离方案主要针对从电子废物中回收金属。
The proposed evaporative separation scheme is mainly targeted to the recovery of metals from e-waste.
尽管如此，它还是可以展现出分离金属的能力。
Nevertheless, it could exhibit the capability for the separation of metals.
理论计算表明，对于大多数蒸汽压差较大的金属，可以实现高达10^5的大分离系数(补充注释4，基于蒸汽压差的蒸发分离过程的理论分离系数，补充图21，补充表3)。
Theoretical calculation shows that large separation factors up to $\sim10^5$ could be realized for most metals with large vapor pressure differences (Supplementary Note 4, theoretical separation factors of the evaporative separation process based on the vapor pressure difference, Supplementary Fig. 21, Supplementary Table 3).
理论分离因子是根据纯金属的蒸气压计算的。
The theoretical separation factors are calculated based on the vapor pressure of pure metals.
它们代表了微量金属分离的实际值，即使在熔融合金形成的情况下也是如此(补充注释4，熔融合金形成对分离系数的影响，补充图22)。
They represent practical values for trace metal separation even with the melt alloy formation (Supplementary Note 4, the effect of melt alloy formation on the separation factors, Supplementary Fig. 22).
贵金属的不同回收率(图1g)已经证明了基于蒸汽压差的FJH工艺的分离可行性(补充注释4，蒸发分离实现的分离能力，补充表4)。
The different recovery yields of precious metals (Fig. 1g) already demonstrated the separation feasibility of the FJH process based on the vapor pressure difference (Supplementary Note 4, the achieved separation ability by the evaporative separation, Supplementary Table 4).
化学添加剂(图2a-f)也调节了贵金属分离，可能是由于其不同的化学反应性(补充注释4，化学添加剂的金属分离能力，补充表5-7)。
The chemical additives (Fig. 2a–f) also regulated the precious metals separation presumably due to their different chemical reactivity (Supplementary Note 4, the metal separation ability from the chemical additives, Supplementary Tables 5–7).
可通过逐步提高FJH温度进一步提高蒸发分离方案的分离能力(补充注释4，基于增加分离系数实践的循证预测)。
The separation ability of the evaporative separation scheme could be further improved by progressively increasing the FJH temperature (Supplementary Note 4, the evidence-based predictions on the practices to increase the separation factors).

对FJH加工的成本和效益进行了评估，因为经济效益是废物回收的主要驱动因素(补充注释5)。
The cost and benefit of the FJH processing were evaluated since economic incentives are the main driver for waste recycling (Supplementary Note 5)[8].
与传统熔炼炉相比，FJH是一种高效的加热工艺，其加热/冷却速度超快，样品直接加热，反应时间短。传统熔炼炉使用大量能量来维持整个炉的温度。
FJH is a highly efficient heating process due to the ultrafast heating/cooling rate, the direct sample heating feature, and the short reaction duration, compared to traditional smelting furnaces where large amounts of energy are used to maintain the temperature of the whole chamber[33].
FJH法的能耗约为939kWh吨，约为实验室规模管式炉的1/500，约为工业规模商用卡尔多炉的1/80(补充注5)。
The FJH method has an energy consumption of ~939 kWh ton^{-1}, which is ~1/500 of that for a lab-scale tubular furnace[34], and ~1/80 of that for a commercially used Kaldo furnace in industrial scale[35] (Supplementary Note 5).
因此，FJH电子废物处理工艺可能比传统的火法冶金工艺具有优势。
Hence, the FJH process for e-waste processing could have advantages over traditional pyrometallurgical processes.

FJH流程具有可扩展性。
The FJH process is scalable.
根据理论分析揭示的标度规律，增大样品质量时，我们可以增加FJH电压和/或电容器组的电容。
According to the scaling rule revealed by the theoretical analysis, we could increase the FJH

(补充注释6和补充图23和24)。通过使用与FJH装置集成的自制自动化系统，我们的研究实验室已经实现了1天10公斤以上的生产能力。FJH工艺的进一步商业规模正在扩大(补充注释6)。考虑到易于获取的贵金属矿石越来越少，以及几种金属元素的毒性，设计的FJH回收电子废物中金属的工艺可能是近期回收方法的原料。

voltage and/or the capacitance of the capacitor bank when scaling up the sample mass (Supplementary Note 6 and Supplementary Figs. 23 and 24). By using a homemade automation system integrated with the FJH setup, our research lab has already realized a production rate of >10 kg day^{-1}. Further commercial scaling up of the FJH process is underway (Supplementary Note 6). Considering the diminishing easily accessible ores of precious metals and the toxicity of several metal elements, the proposed FJH process to recover metals in e-waste could be a harbinger for near-future recovery methods.

方法

Methods

材料 CB(Cabot，Black Pearls 2000，平均直径10 nm)用作导电添加剂。PCB废料来自一台废弃的计算机。使用锯子将PCB切割成小块，然后使用锤式研磨机(Dade，DF-15)将其研磨成微型粉末。盐添加剂为NaCl(J.T.Baker)、NaF(Acros有机物)和NaI(Aldrich，99.5%)。贵金属氯化物为RhCl3(Aldrich，38-40%Rh)、PdCl2(Aldrich，99%)、AgCl(Allied Chemical)和AuCl3(Aldrich，99.9%)。聚四氟乙烯(PTFE)粉末购自Runaway Bike。以管道中的PVC、CPVC和聚偏氟乙烯(PVDF)塑料管为原料。塑料废料用锯子切成小块，然后用锤式粉碎机(Dade，DF-15)研磨成粉末。

Materials. CB (Cabot, Black Pearls 2000, average diameter 10 nm) was used as the conductive additive. The PCB waste was from a discarded computer. The PCB was cut into small pieces using a saw, and then ground into microscale powders by using a hammer grinder (Dade, DF-15). The salt additives were NaCl (J.T. Baker), NaF (Acros Organics), and NaI (Aldrich, 99.5%). The precious metals chlorides were $RhCl_3$ (Aldrich, 38–40% Rh), $PdCl_2$ (Aldrich, 99%), AgCl (Allied Chemical), and $AuCl_3$ (Aldrich, >99.9%). Polytetrafluoroethylene (PTFE) powder was purchased from Runaway Bike. PVC, CPVC, and polyvinylidene fluoride (PVDF) plastic tubes from plumbing pipes were used as raw materials. The plastic waste products were cut into small pieces using a saw, and then ground into powders by using a hammer grinder (Dade, DF-15).

FJH系统和蒸发分离工艺。FJH反应器的电气图见图3。存在触电的风险，因此应仔细遵守所有安全措施，正如我们在补充信息中详细列出的那样。CB、PCB粉末和添加剂通过球磨(MSE Supplies，PMV1-0.4 L)进行混合。将反应物装入内径为8 mm、外径为12 mm的石英管中。在石英管的一侧使用铜棉作为多孔电极以促进气体扩散，在另一侧使用石墨棒作为电极。然后将管加载到反应阶段，并连接到FJH系统。通过压缩电极来控制电阻。石英管由O形圈密封。使用体积约为40 mL的容器作为冷阱。容器应能承受负压(~10Pa)。使用机械泵将容器抽至真空；然后，将捕集器浸入液氮杜瓦瓶中。必须遵循此顺序，以避免N2杜瓦瓶中的O2冷凝，因为O2的沸点高于N2。总电容为60 mF的电容器组由直流(DC)电源充电，电压可达400 V。采用具有可编程ms级延迟时间的继电器控制放电时间。高压放电使样品达到高温。FJH的详细条件见补充表1。对于每种条件，进行了三次FJH实验，以收集总挥发物，用于样品消解和ICP-MS测量。因此，测量的回收率是使用同一电路板进行的三次独立实验的平均值。FJH反应后，允许FJH装置冷却至室温，同时冷阱仍浸没在液态N2中。然后，在仪器保持真空的同时，从液态N2中取出冷阱。冷阱加热至室温后，释放真空。

FJH system and evaporative separation process. The electrical diagram of the FJH reactor is shown in Supplementary Fig. 3. There is a risk of electrocution so all safety measures should be obeyed carefully, as we listed in detail in the Supplementary Information. CB, PCB powders, and additives were mixed by using ball milling (MSE Supplies, PMV1-0.4 L). The reactants were loaded into a quartz tube with an inner diameter of 8 mm and an outer diameter of 12 mm. Copper wool was used as the porous electrode on one side to facilitate the gas diffusion, and a graphite rod was used as the electrode on the other side of the quartz tube. The tube was then loaded on the reaction stage and connected to the FJH system. The resistance was controlled by compressing the electrodes. The quartz tube was sealed by an O-ring. A vessel with a volume of ~40 mL was used as the cold trap. The vessel should withstand negative pressure (~10 Pa). A mechanical pump was used to pump the vessel to vacuum; then, the trap was immersed into the liquid N_2 Dewar. This sequence must be followed to avoid O_2 condensation in the N_2 Dewar since O_2 has a higher boiling point than N_2. A capacitor bank with a total capacitance of 60 mF was charged by a direct current (DC) supply that can reach voltages up to 400 V. A relay with programmable ms-level delay time was used to control the discharge time. The high-voltage discharging brings the sample to a high temperature. The detailed conditions for the FJH are listed in Supplementary Table 1. For each condition, three FJH experiments were conducted to collect the total volatiles for sample digestion and ICP-MS measurement. Hence, the measured recovery yield is the average of three independent experiments using the same circuit board. After the FJH reaction, the FJH apparatus was allowed to cool to room temperature while the cold trap remained immersed in the liquid N_2. Then, the trap was taken out from the liquid N_2 while the apparatus remained under vacuum. After the trap warmed to room temperature, the vacuum was released.

大气压和正压下的FJH。FJH反应类似于蒸发分离，以下变化除外。石英管由O形圈密封以保持压力。多孔铜电极侧通过承受高达5bar压力的管道连接到内部气体(N2)气缸。使用调节器将压力调节至所需值(1 4atm)，并通过压力计进行监测。设定压力后，对FJH系统进行充气，然后排放以进行反应。FJH的详细情况见补充表2。FJH反应后，释放压力，取出样品进行进一步分析。

FJH under atmospheric and positive pressure. The FJH reaction is similar to the evaporative separation except with the following changes. The quartz tube was sealed by an O-ring to hold pressure. The porous Cu electrode side was connected to an inner gas (N_2) cylinder by tubing that withstands pressure up to 5 bar. The pressure was adjusted to the desired values (1–4 atm) using a regulator and was monitored by a pressure gauge. Once the pressure was set, the FJH system was charged and then discharged for reaction. The detailed conditions for the FJH are shown in Supplementary Table 2. After the FJH reaction, the pressure was released, and the sample was removed for further analysis.

表征 SEM图像是在5kV电压下使用FEI Helios NanoLab 660双光束SEM系统获得的。使用配置有Cu K辐射(=1.5406)的Rigaku D/Max Ultima II系统收集XRD。用PHI-Quantera XPS系统在5×109托的基底压力下进行XPS光谱测量。元素XPS光谱使用0.1eV的步长和26 eV的通过能收集。使用284.8 eV的标准C1s峰校准所有XPS光谱。STEM图像和EDS图是在JEOL 2100场发射枪透射电子显微镜上，在通过使用TA仪器的Q-600同时TGA/DSC，在空气中以10 ° Cmin 1至1000 ° C的加热速率进行TGA。使用马弗炉在空气中进行煅烧(NEY 6-160 A)。

Characterization. The SEM images were obtained by using a FEI Helios NanoLab 660 DualBeam SEM system at 5 kV. XRD was collected by using a Rigaku D/Max Ultima II system configured with a Cu Kα radiation ($\lambda = 1.5406$ Å). XPS spectra were taken using a PHI Quantera XPS system under the base pressure of 5×10^{-9} Torr. Elemental XPS spectra were collected using a step size of 0.1 eV with a pass energy of 26 eV. All of the XPS spectra were calibrated by using the standard C 1*s* peak at 284.8 eV. STEM images and EDS maps were taken on a JEOL 2100 Field Emission Gun Transmission Electron Microscope under the voltage of 200 kV. TGA was conducted in air at a heating rate of 10 °C min^{-1} up to 1000 °C by using a Q-600 Simultaneous TGA/DSC from TA instruments. Calcination was conducted using the Mafu furnace in the air (NEY 6-160 A).

样品消解和ICP-MS测量。购买标准来自Millipore Sigma。使用三种元素周期表混合物和汞标准，其中成分列于补充表8中。样品消解使用HNO3(67-70 wt%，TraceMetalTM级，费希尔化学)、HCl(37 wt%，99.99%微量金属基，Millipore-Sigma)和水(Millipore-Sigma，ACS超痕量分析试剂)。使用稀释王水法溶解样品。样品在45 ° C的HNO3/HCl(各1M)溶液中浸泡24小时。过滤酸性溶液以去除任何未溶解的颗粒。然后在校准曲线内使用2wt%HNO3或HCl将溶液稀释至适当的浓度范围。ICP-MS使用Perkin Elmer Nexion 300 ICP-MS系统进行。PCB原料粉末、来自冷阱的冷凝固体、PCB闪蒸粉末、PCB闪蒸煅烧粉末和PCB煅烧粉末使用相同的方案进行浸出。

Sample digestion and ICP-MS measurement. The standards were purchased from Millipore-Sigma. Three periodic table mixtures and Hg standard were used, where the composition is listed in Supplementary Table 8. HNO_3 (67–70 wt%, TraceMetal^{TM} Grade, Fisher Chemical), HCl (37 wt%, 99.99% trace metals basis, Millipore-Sigma), and water (Millipore-Sigma, ACS reagent for ultratrace analysis) were used for sample digestion. The samples were digested by using a diluted aqua regia method[14,19]. The samples were soaked in HNO_3/HCl (1 M each) solution at 45 °C for 24 h. The acidic solution was filtered to remove any undissolved particles. The solution was then diluted to the appropriate concentration range using 2 wt% HNO_3 or HCl within the calibration curve. ICP-MS was conducted using a Perkin Elmer Nexion 300 ICP-MS system. The PCB raw powder, the condensed solid from the cold trap, the PCB-Flash powder, the PCB-Flash-Calcination powder, and the PCB-Calcination powder were leached using the same protocol.

Data availability

The data supporting the findings of this study are available within the article and its Supplementary Information. Other relevant data are available from the corresponding author upon reasonable request. Source data generated in this study are provided in the Source Data file. The Source Data file is also uploaded to the Zenodo repository https://doi.org/10.5281/zenodo.5293916. Source data are provided with this paper.

Received: 4 May 2021; Accepted: 7 September 2021;

References

1. Zhang, K., Schnoor, J. L. & Zeng, E. Y. E-waste recycling: where does it go from here? *Environ. Sci. Technol.* **46**, 10861–10867 (2012).
2. Zeng, X. L., Mathews, J. A. & Li, J. H. Urban mining of e-waste is becoming more cost-effective than virgin mining. *Environ. Sci. Technol.* **52**, 4835–4841 (2018).
3. Ogunseitan, O. A., Schoenung, J. M., Saphores, J.-D. M. & Shapiro, A. A. The electronics revolution: From e-wonderland to e-wasteland. *Science* **326**, 670–671 (2009).
4. Wang, Z. H., Zhang, B. & Guan, D. B. Take responsibility for electronic-waste disposal. *Nature* **536**, 23–25 (2016).
5. Ghosh, B., Ghosh, M. K., Parhi, P., Mukherjee, P. S. & Mishra, B. K. Waste printed circuit boards recycling: an extensive assessment of current status. *J. Clean. Prod.* **94**, 5–19 (2015).
6. Leung, A. O. W., Duzgoren-Aydin, N. S., Cheung, K. C. & Wong, M. H. Heavy metals concentrations of surface dust from e-waste recycling and its human health implications in southeast China. *Environ. Sci. Technol.* **42**, 2674–2680 (2008).
7. Julander, A. et al. Formal recycling of e-waste leads to increased exposure to toxic metals: an occupational exposure study from Sweden. *Environ. Int.* **73**, 243–251 (2014).
8. Awasthi, A. K., Li, J. H., Koh, L. & Ogunseitan, O. A. Circular economy and electronic waste. *Nat. Electron.* **2**, 86–89 (2019).
9. Kaya, M. Recovery of metals and nonmetals from electronic waste by physical and chemical recycling processes. *Waste Manag.* **57**, 64–90 (2016).
10. Popoola, O. E., Popoola, A. O. & Purchase, D. Levels of awareness and concentrations of heavy metals in the blood of electronic waste scavengers in Nigeria. *J. Health Pollut.* **9**, 190311 (2019).
11. Hall, W. J. & Williams, P. T. Separation and recovery of materials from scrap printed circuit boards. *Resour. Conserv. Recy.* **51**, 691–709 (2007).
12. Cui, J. R. & Zhang, L. F. Metallurgical recovery of metals from electronic waste: a review. *J. Hazard. Mater.* **158**, 228–256 (2008).
13. Sun, Z. et al. Toward sustainability for recovery of critical metals from electronic waste: the hydrochemistry processes. ACS Sustain. *Chem. Eng.* **5**, 21–40 (2017).
14. Jadhav, U. & Hocheng, H. C. Hydrometallurgical recovery of metals from large printed circuit board pieces. *Sci. Rep.* **5**, 14574 (2015).
15. Zhuang, W. Q. et al. Recovery of critical metals using biometallurgy. *Curr. Opin. Biotech.* **33**, 327–335 (2015).
16. Sarvar, M., Salarirad, M. M. & Shabani, M. A. Characterization and mechanical separation of metals from computer printed circuit boards (PCBs) based on mineral processing methods. *Waste Manag.* **45**, 246–257 (2015).
17. Yamane, L. H., de Moraes, V. T., Espinosa, D. C. R. & Tenorio, J. A. S. Recycling of WEEE: characterization of spent printed circuit boards from mobile phones and computers. *Waste Manag.* **31**, 2553–2558 (2011).
18. Sethurajan, M. et al. Recent advances on hydrometallurgical recovery of critical and precious elements from end of life electronic wastes-a review. *Crit. Rev. Env. Sci. Tec.* **49**, 212–275 (2019).
19. Hong, Y. et al. Precious metal recovery from electronic waste by a porous porphyrin polymer. *Proc. Natl Acad. Sci. USA* **117**, 16174–16180 (2020).
20. Abrahamson, J. Graphite sublimation temperatures, carbon arcs and crystalline erosion. *Carbon* **12**, 111–141 (1974).

21. Luong, D. X. et al. Gram-scale bottom-up flash graphene synthesis. *Nature* **577**, 647–651 (2020).
22. Algozeeb, W. A. et al. Flash graphene from plastic waste. *ACS Nano* **14**, 15595–15604 (2020).
23. Okamoto, H., Schlesinger, M. E. & Mueller, E. M. *ASM Handbook Volume 3: Alloy Phase Diagrams*. (ASM International, 2016).
24. Lide, D. R. *CRC Handbook of Chemistry and Physics*, Ch. 4 (CRC Press, Internet Version, 2005).
25. Pearson, R. G. Hard and soft acids and bases. *J. Am. Chem. Soc.* **85**, 3533–3539 (1963).
26. Ueda, T., Ichiishi, S., Okuda, A. & Matsutani, K. *Metal Sustainability: Global Challenges, Consequences, and Prospects*, Ch. 15 (John Wiley & Sons Press, 2016).
27. Yao, Y. G. et al. Carbothermal shock synthesis of high-entropy-alloy nanoparticles. *Science* **359**, 1489–1494 (2018).
28. Olavarria-Contreras, I. J. et al. C-Au covalently bonded molecular junctions using nonprotected alkynyl anchoring groups. *J. Am. Chem. Soc.* **138**, 8465–8469 (2016).
29. Park, Y. J. & Fray, D. J. Recovery of high purity precious metals from printed circuit boards. *J. Hazard. Mater.* **164**, 1152–1158 (2009).
30. Quinet, P., Proost, J. & Van Lierde, A. Recovery of precious metals from electronic scrap by hydrometallurgical processing routes. *Miner. Metall. Proc.* **22**, 17–22 (2005).
31. Sun, G. L., Reynolds, E. E. & Belcher, A. M. Using yeast to sustainably remediate and extract heavy metals from waste waters. *Nat. Sustain.* **3**, 303–311 (2020).
32. Kinuthia, G. K. et al. Levels of heavy metals in wastewater and soil samples from open drainage channels in Nairobi, Kenya: community health implication. *Sci. Rep.* **10**, 8434 (2020).
33. Khaliq, A., Rhamdhani, M. A., Brooks, G. & Masood, S. Metal extraction processes for electronic waste and existing industrial routes: a review and Australian perspective. *Resources* **3**, 152–179 (2014).
34. Balaji, R. & Senophiyah-Mary, J. *Urban Mining and Sustainable Waste Management*, Ch. 7 (Springer, 2020).
35. Theo, L. Integrated recycling of non-ferrous metals at Boliden Ltd. Ronnskar smelter. in *Proceedings of the 1998 IEEE International Symposium on Electronics and the Environment. ISEE - 1998 (Cat. No. 98CH36145)* 42–47 (IEEE, 1998).

Acknowledgements

We acknowledge Dr. Helge Gonnermann of Rice University for allowing us to use the FEM simulation software. We acknowledge Dr. Bo Chen of Rice University for the helpful discussion of the XPS results. The funding of the research is provided by the Air Force Office of Scientific Research (FA9550-19-1-0296) and the Department of Energy, DOE-NETL (DE-FE0031794). The authors acknowledge the use of the Electron Microscopy Center (EMC) at Rice University. This work was conducted in part using resources of the Shared Equipment Authority (SEA) at Rice University.

Author contributions

B.D. and J.M.T. conceived the idea to use FJH to recover metals. B.D. conducted most of the experimental work with the help of Z.W., E.A.M. helped with the ICP-MS, and C.K. and D.X.L. designed and built the FJH system and the temperature measurement setup. B.D. and J.M.T. wrote the manuscript. All aspects of the research were overseen by J.M.T. All authors discussed the results and commented on the manuscript.

Competing interests

Rice University owns intellectual property on the FJH strategy for urban mining, and a patent application has been filed. The scaling of the FJH process for the production of graphene (not considered in the research described here) is licensed by Universal Matter Inc. and Universal Matter Ltd. from Rice University. J.M.T. owns stock in these companies, but he is not an officer or director therein. All conflicts of interest are managed through regular disclosure to the Rice University Office of Sponsored Programs and Research Compliance.

Additional information

Supplementary information The online version contains supplementary material available at https://doi.org/10.1038/s41467-021-26038-9.

Correspondence and requests for materials should be addressed to James M. Tour.

Peer review information *Nature Communications* thanks the anonymous reviewer(s) for their contribution to the peer review of this work.